

Microscopic mechanism of unusual lattice thermal transport in TlInTe_2

Koushik Pal,^{1,*} Yi Xia,¹ and Chris Wolverton^{1,†}

¹*Department of Materials Science and Engineering, Northwestern University, Evanston, IL 60208, USA*

We investigate the microscopic mechanism of ultralow lattice thermal conductivity (κ_l) of TlInTe_2 and its weak temperature dependence using a unified theory of lattice heat transport that considers contributions arising from the particle-like propagation as well as wave-like tunneling of phonons. While we use the Peierls-Boltzmann transport equation (PBTE) to calculate the particle-like contributions ($\kappa_l(\text{PBTE})$), we explicitly calculate the off-diagonal (OD) components of the heat-flux operator within a first-principles density functional theory framework to determine the contributions ($\kappa_l(\text{OD})$) arising from the wave-like tunneling of phonons. At each temperature, T , we anharmonically renormalize the phonon frequencies using the self-consistent phonon theory including quartic anharmonicity, and utilize them to calculate $\kappa_l(\text{PBTE})$ and $\kappa_l(\text{OD})$. With the combined inclusion of $\kappa_l(\text{PBTE})$, $\kappa_l(\text{OD})$, and additional grain-boundary scatterings, our calculations successfully reproduce the experimental results. Our analysis shows that large quartic anharmonicity of TlInTe_2 (a) strongly hardens the low-energy phonon branches, (b) diminishes the three-phonon scattering processes at finite T , and (c) recovers the weaker than T^{-1} decay of the measured κ_l .

INTRODUCTION

Crystalline semiconductors with ultralow lattice thermal conductivity (κ_l) are important for effective utilization and management of thermal energy in high-performance thermoelectrics [1–4], photovoltaics [5–8], thermal barrier coatings [9], and thermal data storage devices [10]. Although it is quite natural for compounds with complex crystal structures having large unit cells [11, 12] and heavy atoms to exhibit low- κ_l , relatively simple crystalline materials having small unit cells and even with light atoms [13] could also possess ultralow- κ_l due to the presence of rattler atoms [14], strong lattice anharmonicity [15–19], or bonding heterogeneity [20–23]. Investigation of the microscopic mechanism behind the ultralow- κ_l that often approaches the glassy limit in ordered compounds is not only fundamentally interesting, but it also helps to unravel the complex correlation between the crystal structure, bonding, and anharmonic lattice dynamics. Results of such investigations provide new criteria to find hitherto unknown low- κ_l materials as well as paves the way to engineer the heat transport properties in already known compounds.

Despite significant research efforts, a comprehensive theoretical understanding of the mechanism behind extremely poor heat transport in ultralow- κ_l materials, which approach the limit of their theoretical minimum (κ_{min}) has remained challenging [24–26]. This is in part due to the fact that many of these materials are often so highly anharmonic that a harmonic description of the phonon frequencies fails to describe the lattice dynamics of the compounds correctly. Hence, a finite temperature treatment of the phonon modes becomes necessary to

account for the renormalization of the phonon frequencies arising from the temperature induced anharmonic effects. In some cases, the mean free paths of the phonon modes approach the smallest atomic distance in the crystal, leading to a breakdown of the conventional particle-like description of phonons towards a glass-like thermal conductivity [27]. However, recent theoretical and computational developments [28–33] have enabled the treatment of phonons at finite temperature considering anharmonicity arising from high-order phonon-phonon interactions, and examination beyond the particle-like description by including the contributions arising from the wave-like tunneling of phonons [32, 33]. In recent theoretical studies, it was shown that the ultralow κ_l in many well known family of crystalline solids such as clathrates [30], double-halide perovskites [34], tetrahedrites [35], Tl_3VSe_4 [36] can only be explained successfully if higher-order anharmonic phonon-phonon interactions are taken into account in the description of their lattice dynamics and phonon transport [29, 37].

In this work, we develop a microscopic understanding and uncover the physical principles underlying the unusual lattice thermal transport properties of TlInTe_2 which exhibits ultralow- κ_l that is close to its theoretical minimum [38, 39] and shows weak (milder than T^{-1} decay) temperature dependence in κ_l . TlInTe_2 represents a class of structurally similar ABX_2 ($\text{A}=\text{Tl}^{1+}$, In^{1+} ; $\text{B}=\text{Tl}^{3+}$, In^{3+} , Ga^{3+} ; $\text{X}=\text{Se}^{2-}$, Te^{2-}) compounds, many of which are shown to exhibit ultralow- κ_l due to the presence of rattler cation at the A-site [38–41]. The rattler cations manifest nearly dispersion-less optical phonon branches at low-energies which effectively scatter the heat-carrying phonons by creating additional phonon scattering channels [18, 42, 43]. Since phonon scattering rates crucially depend on the phonon frequencies [44] and the rattling phonon modes are quite sensitive to temperature, an accurate treatment of the thermal transport properties in the above compounds requires the treat-

* koushik.pal.physics@gmail.com

† c-wolverton@northwestern.edu

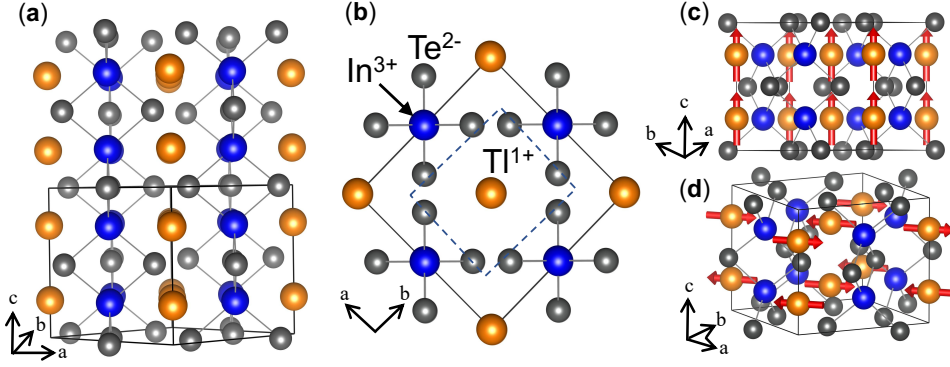


FIG. 1. Crystal structure, bonding, and rattling vibrations. (a) Chain-like crystal structure of TlInTe_2 , where In^{3+} cations (blue sphere) are tetrahedrally coordinated by Te^{2-} anions (dark grey sphere), forming InTe_4 tetrahedron. These InTe_4 tetrahedra share their edges, and extend along the c -axis, giving rise to a chain-like structure. Tl^{1+} cations (orange sphere) occupy the spaces between the chains and stabilize the structure through electron transfer from Tl^{1+} to the $[\text{InTe}_2]^{1-}$ sublattices. The conventional unit cell is outlined by the solid black line. (b) A top-down view of the crystal structure, where it can be seen that Tl atom occupies the empty space inside the square anti-prismatic (outlined by dashed blue line) environment formed by eight Te atoms. Visualization of the (c) longitudinal (R_{LO}) and (d) transverse (R_{TO}) optical rattling (R) phonon modes at the X point in the Brillouin zone, where the atomic displacements are indicated by the red arrows.

ment of phonons at finite temperature including anharmonic effects [29, 45]. However, a comprehensive theoretical understanding of the lattice thermal transport including the effects of temperature-induced anharmonic renormalizations to the phonon frequencies is missing in this family of compounds. Here, we use a unified theory of lattice thermal conductivity that considers the contributions arising from the particle-like propagation as well as wave-like tunneling of phonons. We utilize the phonon frequencies that are renormalized at finite temperatures including the effects of quartic anharmonicity to calculate both these contributions to κ_l .

The particle-like contributions ($\kappa_l(\text{PBTE})$) which are obtained after solving the Peierls-Boltzmann transport equation (PBTE) only account for the diagonal components of the heat-flux operator [32, 46–48]: $J^\alpha = -\kappa_l^{\alpha\beta} \nabla T^\beta$, where ∇T is the temperature gradient and α, β are the Cartesian coordinates. We also calculate the off-diagonal (OD) contributions, $\kappa_l(\text{OD})$, associated with the OD components of the heat-flux operator, which are not present in the PBTE formalism. $\kappa_l(\text{OD})$ is related to the wave-like tunneling of phonons, which is the heat carried by the coupled vibrational eigenstates as a result of the loss of coherence between them [32, 33, 46, 49]. In a recent theoretical work, Simoncelli et al. [32] combined both the pictures (i.e., particle-like and wave-like) of phonon transport in a unified theory of lattice heat transport, where the total κ_l is given by $\kappa_l^{\alpha\beta}(\text{tot}) = \kappa_l^{\alpha\beta}(\text{PBTE}) + \kappa_l^{\alpha\beta}(\text{OD})$, which successfully describes the κ_l of anharmonic crystals, harmonic glasses as well as complex compounds such as tetrahedrites [32, 35, 36]. Our calculated κ_l within the PBTE formalism in conjunction with the OD contributions using the renormal-

ized phonon frequencies, and additional grain-boundary scatterings successfully reproduce two sets of available experimental results [38, 39] of TlInTe_2 . Our analysis reveals that TlInTe_2 possesses large quartic anharmonicity that (a) strongly hardens the low-energy rattling and other optical phonon branches with temperature, (b) diminishes the three-phonon scattering rates at finite temperatures, and (c) recovers the magnitude as well as the correct T -dependence of κ_l that shows weaker than T^{-1} decay found in experimental measurements.

RESULTS

Crystal structure and anharmonicity

TlInTe_2 has a chain-like body-centered tetragonal (space group: $I4/mcm$) crystal structure (Fig. 1a) with eight atoms in the primitive unit cell. Within the unit cell, In^{3+} cations are covalently bonded to four Te atoms, forming the InTe_4 tetrahedra which share their edges and extend like chains along the crystallographic c -axis. The empty spaces between these chains are bridged by the Tl atoms which stabilize the structure through electron transfer from Tl^{1+} cation to the $[\text{InTe}_2]^{1-}$ anion sublattices. Analysis of the second-order interatomic force constants (IFCs) reveals that In^{3+} are strongly bonded to the lattice, whereas the Tl^{1+} cations are only loosely connected (see Supplementary Figure 2). In the crystal structure, Tl atoms are coordinated by eight Te atoms in a square anti-prismatic coordination environment (Fig. 2b) forming an oversized cage (also known as Thompson cube) inside which the Tl atoms rattle due to their weaker

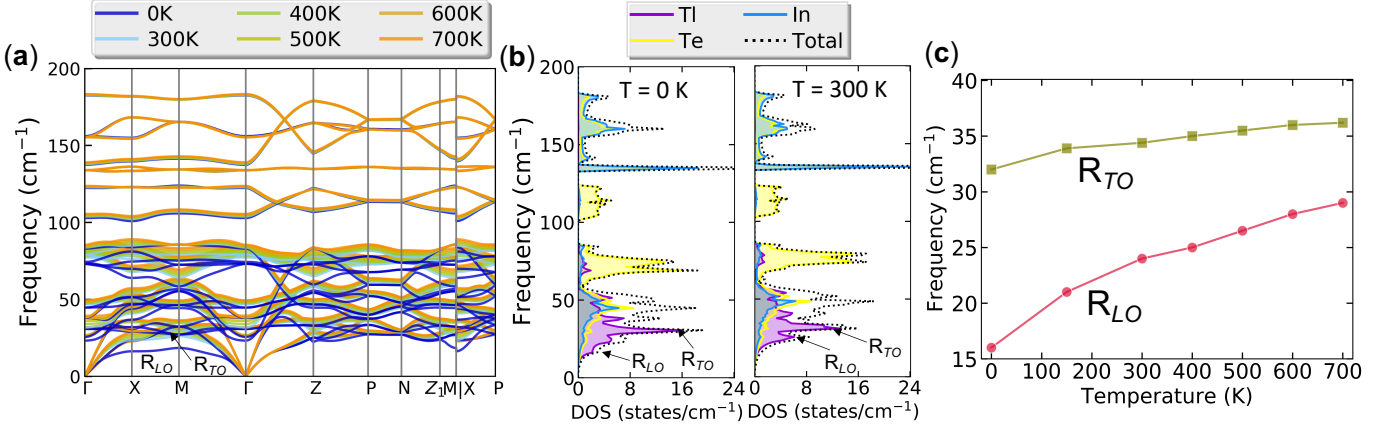


FIG. 2. Temperature-induced anharmonic phonon renormalization. (a) Anharmonically renormalized phonon dispersions of TlInTe₂ at finite temperatures (0-700 K). The longitudinal optical (R_{LO}) and transverse optical (R_{TO}) rattling phonon branches at T = 0 K are marked with arrows. (b) Atom-resolved phonon density of states of TlInTe₂ at 0 K and 300 K, where the peaks associated with the R_{LO} and R_{TO} phonons are indicated. (c) Variations of the R_{LO} and R_{TO} modes at the X-point in the Brillouin zone as a function of temperature.

chemical bonding. The rattling (R) vibrations have two components: (a) the longitudinal optical (R_{LO}) and (b) transverse optical (R_{TO}) branches, which are shown in Fig. 1c and Fig. 1d, respectively. As will be discussed later, the R_{LO} branch is strongly affected by the temperature, which suppresses the phonon-scattering rates at high temperature, giving rise to a milder $T^{-0.86}$ decay of the calculated κ_l that is closer to the temperature dependence of $T^{-0.88}$ and $T^{-0.82}$ found in the experimentally measured κ_l of TlInTe₂ in two sets of experiments [38, 39].

Since the presence of strong anharmonicity is an important characteristic of many ultralow- κ_l compounds, it is necessary to assess its strength in TlInTe₂. Anharmonicity of the phonon modes is estimated by the mode Gruniesen parameters ($\gamma_\lambda = -\frac{d\ln\omega_\lambda}{d\ln V}$) that quantify the change of the phonon frequencies (ω_λ) with respect to the change in the unit cell volume (V), where λ is a composite index that combines the wave vector (q) and phonon branch index (s). While for weakly anharmonic solids γ_λ 's are close to 1, for highly anharmonic materials γ_λ 's become much larger than 1. Some examples of compounds that possess large γ_λ 's (hence, strong anharmonicity) and ultralow- κ_l are AgBiSe₂ [16] and SnSe [15, 50]. Previous studies [39–41, 51] have shown that the phonon modes of this ABX₂ family of materials exhibit large γ_λ 's. Thus, in the presence of strong anharmonicity, the harmonic description of the phonon frequencies of the compounds in this family becomes inappropriate at finite temperatures as the anharmonicity induces multi-phonon interactions, giving rise to shifts in the phonon frequencies and broadening of the phonon states. As a

consequence, the phonon frequencies of these anharmonic solids are expected to have strong renormalization effects at finite temperatures, which can crucially alter both the magnitude and T-dependence of the κ_l that deviates from the ideal T^{-1} behavior found in weakly anharmonic solids. Indeed, the weak temperature dependence of the experimentally measured [38, 39] κ_l of TlInTe₂, which decays as $T^{-0.88}$ and $T^{-0.82}$, signifies the prevalence of severe anharmonicity in the crystal structure of TlInTe₂.

Temperature-induced anharmonic phonon renormalization

We use the self-consistent phonon theory (SCPH) [29, 31, 52, 53] to renormalize the phonon frequencies of TlInTe₂ at finite temperatures including anharmonic effects [28] which are treated as the phonon self-energies [31, 54]. Within the SCPH theory, the anharmonically renormalized phonon frequency is determined from the pole of the many-body Green's function. Considering only the first-order contribution to the phonon self-energy arising from the quartic anharmonicity, the SCPH equation [29] is written as $\Omega_\lambda^2 = \omega_\lambda^2 + 2\Omega_\lambda I_\lambda$, where ω_λ is the harmonic phonon frequency at T = 0 K and Ω_λ is the anharmonically renormalized phonon frequency at finite T. The quantity I_λ is defined as: $I_\lambda = \frac{\hbar}{8N} \sum_{\lambda_1} \frac{V^{(4)}(\lambda, -\lambda, \lambda_1, -\lambda_1)}{\Omega_\lambda \Omega_{\lambda_1}} [1 + 2n(\Omega_{\lambda_1})]$, where N , \hbar , n , and $V^{(4)}(\lambda, -\lambda, \lambda_1, -\lambda_1)$ are the number of sampled wave vectors, the reduced Planck constant, the temperature-dependent phonon population, and the reciprocal representation of the fourth-order IFCs, respec-

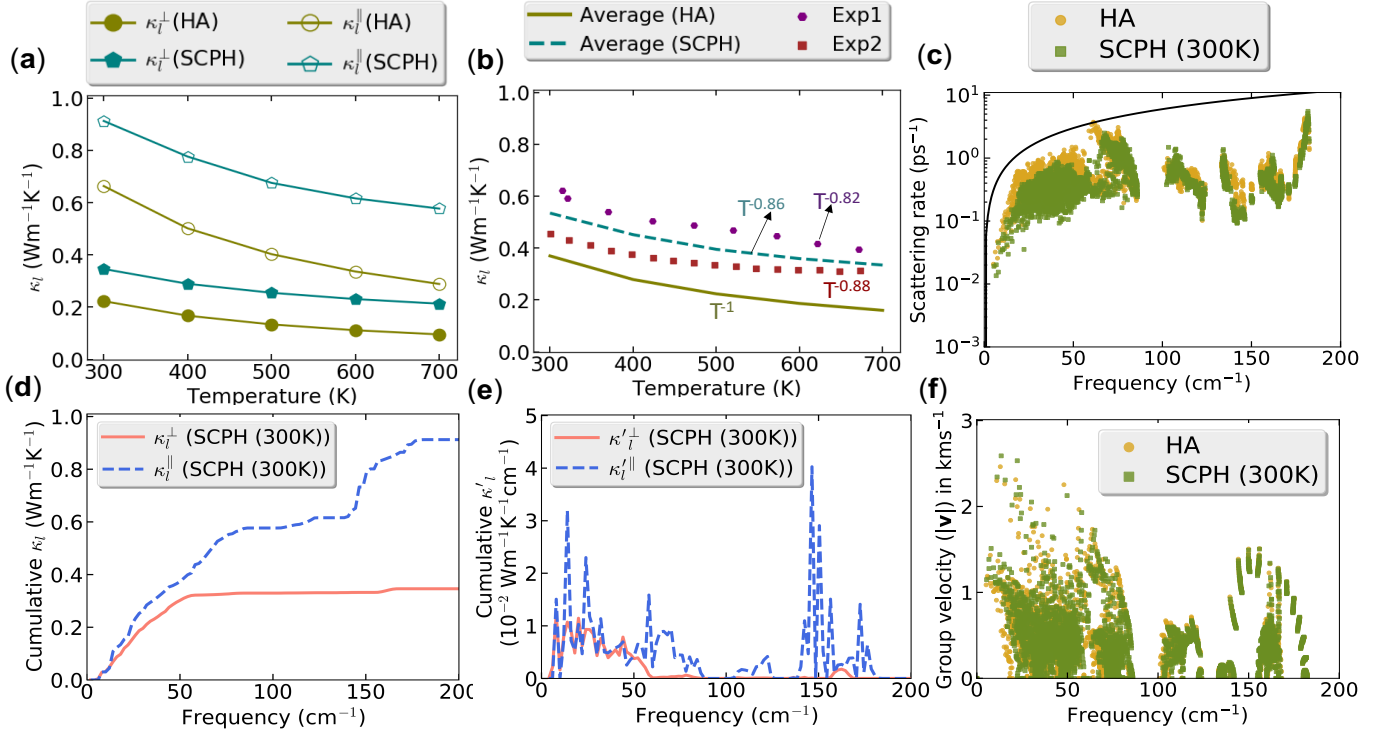


FIG. 3. Heat transport due to particle-like propagation of phonons. (a) Particle-like contributions to the lattice thermal conductivity (κ_l) of TlInTe₂ calculated utilizing the harmonic (i.e., HA) and the anharmonically renormalized (i.e., SCPH) phonon frequencies using the PBTE. κ_l^{\parallel} and κ_l^{\perp} are the components of κ_l , which are parallel and perpendicular to the chain directions in the crystal structure of TlInTe₂, respectively. (b) The averages of the κ_l^{\parallel} and κ_l^{\perp} components are compared against the experimentally measured values which are denoted with Exp1 and Exp2 taken from Ref. [38] and Ref. [39], respectively. (c) Three-phonon scattering rates, and (f) phonon group velocities rates obtained using the harmonic (i.e., HA) and anharmonically renormalized (i.e., SCPH) phonon frequencies at $T = 300$ K. Mode contributions to κ_l^{\parallel} and κ_l^{\perp} are analyzed through (d) the cumulative plots and (e) their first-order derivatives with respect to the anharmonically renormalized phonon frequency at $T = 300$ K. The solid black line in (c) assumes the scattering rates of the phonon modes to be twice their frequencies according to the Cahill-Watson-Pohl model [24].

tively. The temperature dependence of the SCPH equation is contained in the phonon population term that obeys the Bose-Einstein statistics. Since Ω_λ and I_λ are inter-dependent on each other, the SCPH equation is solved self-consistently until the convergence in Ω_λ is achieved.

We present the anharmonically renormalized phonon dispersions of TlInTe₂ in Fig. 2a in the temperature range between 0-700 K. The harmonic phonon dispersion (i.e., $T = 0$ K) of TlInTe₂ exhibits two groups of low-frequency optical phonon branches with very small dispersions, that are characteristic of the rattler atoms in the crystal structure. The lowest-energy rattling phonon branch (denoted as R_{LO}) arises from the longitudinal vibration of Tl¹⁺ ions along the direction of the InTe₄ chains (Fig. 1c) inside the hollow Thompson cube. The second group of rattling phonon branches (R_{TO}) appears above R_{LO} , where the Tl¹⁺ cations vibrate along the transverse direction (i.e., perpendicular to the InTe₄ chains, Fig. 1d). Both R_{LO} and R_{TO} phonons are highly

localized at $T = 0$ K as revealed by analysis based on the phonon participation ratio [42, 55], which does not change as they are anharmonically renormalized at finite temperatures (see Supplementary Figure 6 and Supplementary Note 4). The atom-resolved phonon density of states at $T = 0$ and $T = 300$ K are shown in Fig. 2b, which clearly show the two peaks associated with R_{LO} and R_{TO} phonons, which gradually convolute as the temperature increases. It is seen from Fig. 2a that only the phonons up to 100 cm⁻¹ are strongly hardened while the phonons above 100 cm⁻¹ show very weak hardening or softening. The most drastic temperature-induced changes are observed in the frequency hardening of R_{LO} and R_{TO} phonons (Fig. 2c). It is interesting to note that the frequency of R_{LO} phonon is smaller than that of R_{TO} due to the chain-like crystal structure and weak bonding of Tl atoms which vibrate slowly but with much larger amplitudes along the c -direction in the empty space within the lattice.

Particle-like contributions to κ_l

We start our analysis of the thermal conductivity by examining the calculated κ_l obtained from solving the PBTE using the harmonic (i.e., $T = 0$ K) and anharmonically renormalized phonon frequencies (at finite T) obtained using the SCPH method. Hereafter, we denote these results by $\kappa_l(\text{HA})$, and $\kappa_l(\text{SCPH})$, respectively, as shown in Fig. 3a. It is seen that $\kappa_l(\text{HA})$ changes significantly when the renormalized phonon frequencies are incorporated. For example, $\kappa_l^\perp(\text{HA})$ and $\kappa_l^\parallel(\text{HA})$ increase by 55 % and 38 %, respectively, at 300 K when the renormalized phonon frequencies are used to solve the PBTE. Here, \parallel and \perp symbols indicate components of κ_l parallel and perpendicular to the chain direction (i.e., the c -axis) in the crystal structure of TlInTe_2 , respectively. We compare the average κ_l calculated under both HA and SCPH methods with that of available experimental measurements [38, 39] of κ_l in TlInTe_2 . From Fig. 3b, we see that the average $\kappa_l(\text{HA})$ is significantly underestimated in magnitude compared to the two sets of available experiments [38, 39]. While $\kappa_l(\text{HA})$ decays as T^{-1} according to well-known behavior of the lattice thermal conductivity found in weakly anharmonic solids, the two experimentally measured κ_l data decay as $T^{-0.82}$ and $T^{-0.88}$. The deviation from T^{-1} behavior and the weaker temperature dependence signify the presence of a strong higher-order anharmonicity in TlInTe_2 , and thus necessitate the anharmonic renormalization of the harmonic phonon frequencies. The calculated average of κ_l within the SCPH method increases in magnitude with respect to $\kappa_l(\text{HA})$, but still does not agree well with either sets of experimentally measured values of κ_l . However, the effect of anharmonic renormalization significantly improves the temperature dependence, which varies as $T^{-0.86}$ (Fig. 3b), bringing it closer to the experimental observations.

Next, we analyze how the anharmonic renormalization affects the two key ingredients that enter into the PBTE (see Supplementary Note 2), namely the three-phonon scattering rates (Fig. 3c) and the phonon group velocities (Fig. 3f). According to the phonon gas model, where the phonons behave like particles, the maximum phonon scattering rate of a phonon mode is assumed to be twice its frequency [24], which is denoted with a black line in Fig. 3c. The HA scattering rates are strongly suppressed by the anharmonic effects in the frequency region below 100 cm^{-1} which enhances the phonon lifetimes, leading to a large increase in $\kappa_l(\text{SCPH})$ compared to $\kappa_l(\text{HA})$. The SCPH scattering rates are well below the solid black line, indicating the dominant particle-like nature of the phonons in TlInTe_2 that rules out the existence of a hopping channel of instantaneously localized vibrations as shown in Ref. [51]. The phonon group velocities are weakly hardened below 100 cm^{-1} (Fig. 3f) due to the anharmonic effects at finite temperatures and its effect

on $\kappa_l(\text{SCPH})$ is less significant than that of the scattering rates. To examine the phonon mode specific contributions to κ_l , we show the cumulative plot of $\kappa_l(\text{SCPH})$, and its derivative $\kappa_l'(\text{SCPH})$ with respect to renormalized phonon frequency in Fig. 3d and Fig. 3e, respectively. The cumulative plot for κ_l^\perp changes rapidly up to 60 cm^{-1} and reaches a plateau above it, showing that only the acoustic and low-energy optical phonons mainly contribute to it. This is also clear from Fig. 3e, where large peaks are present mainly up to 60 cm^{-1} . On the other hand, examining κ_l^\parallel in both Fig. 3e and Fig. 3f, reveals that κ_l^\parallel has large contributions coming not only from the acoustic and low-energy optical phonons ($< 80 \text{ cm}^{-1}$) but also from the high-energy optical phonons ($\sim 140\text{--}180 \text{ cm}^{-1}$).

Off-diagonal contributions to κ_l

To understand the difference between the measured κ_l and calculated κ_l (within the SCPH method) of TlInTe_2 , we recognize that κ_l obtained after solving the PBTE i.e., $\kappa_l(\text{PBTE})$ only accounts for the diagonal components of the heat-flux operator [32, 47, 48]. We calculate the off-diagonal (OD) contributions i.e., $\kappa_l(\text{OD})$ using the renormalized phonon frequencies and obtain the total [32] κ_l as: $\kappa_l(\text{tot}) = \kappa_l(\text{PBTE}) + \kappa_l(\text{OD})$ (see Supplementary Note 1). It was shown that while $\kappa_l(\text{OD})$ is negligible in compounds like Si and diamond, while it is very important in CsPbBr_3 and tetrahedrites [32, 35, 36, 46]. One key quantity that enters into the expressions for $\kappa_l(\text{PBTE})$ and $\kappa_l(\text{OD})$ is the generalized phonon group velocity operator (see its expression in SI), \mathbf{V}_{s_1, s_2} , where s_1 and s_2 are phonon branch indices. While $\kappa_l(\text{PBTE})$ utilizes only the diagonal components (i.e., $s_1 = s_2$) of \mathbf{V}^{s_1, s_2} , the $\kappa_l(\text{OD})$ term uses the off-diagonal (i.e., $s_1 \neq s_2$) components of \mathbf{V}^{s_1, s_2} . Fig. 4a shows the κ_l^\perp and κ_l^\parallel components of $\kappa_l(\text{OD})$, and their average as a function of temperature. Although on an absolute scale these values are small, for low- κ_l compounds, these values are quite significant. For example at 300K, $\kappa_l^\perp(\text{OD})$ and $\kappa_l^\parallel(\text{OD})$ account for 14 % and 10 % contributions to that of $\kappa_l^\perp(\text{SCPH})$ and $\kappa_l^\parallel(\text{SCPH})$ values, respectively. However, with increasing temperature, the relative OD contributions also increase. For example, the contributions of $\kappa_l^\perp(\text{OD})$ and $\kappa_l^\parallel(\text{OD})$ increase to 26 % and 15 %, respectively at 700 K. When the average $\kappa_l(\text{OD})$ is added on top of the average $\kappa_l(\text{SCPH})$ terms, the resulting κ_l agrees very well both in magnitude with one set of experiments, Exp1 [38] and in temperature dependence that decays as $T^{-0.80}$ (Fig. 4b).

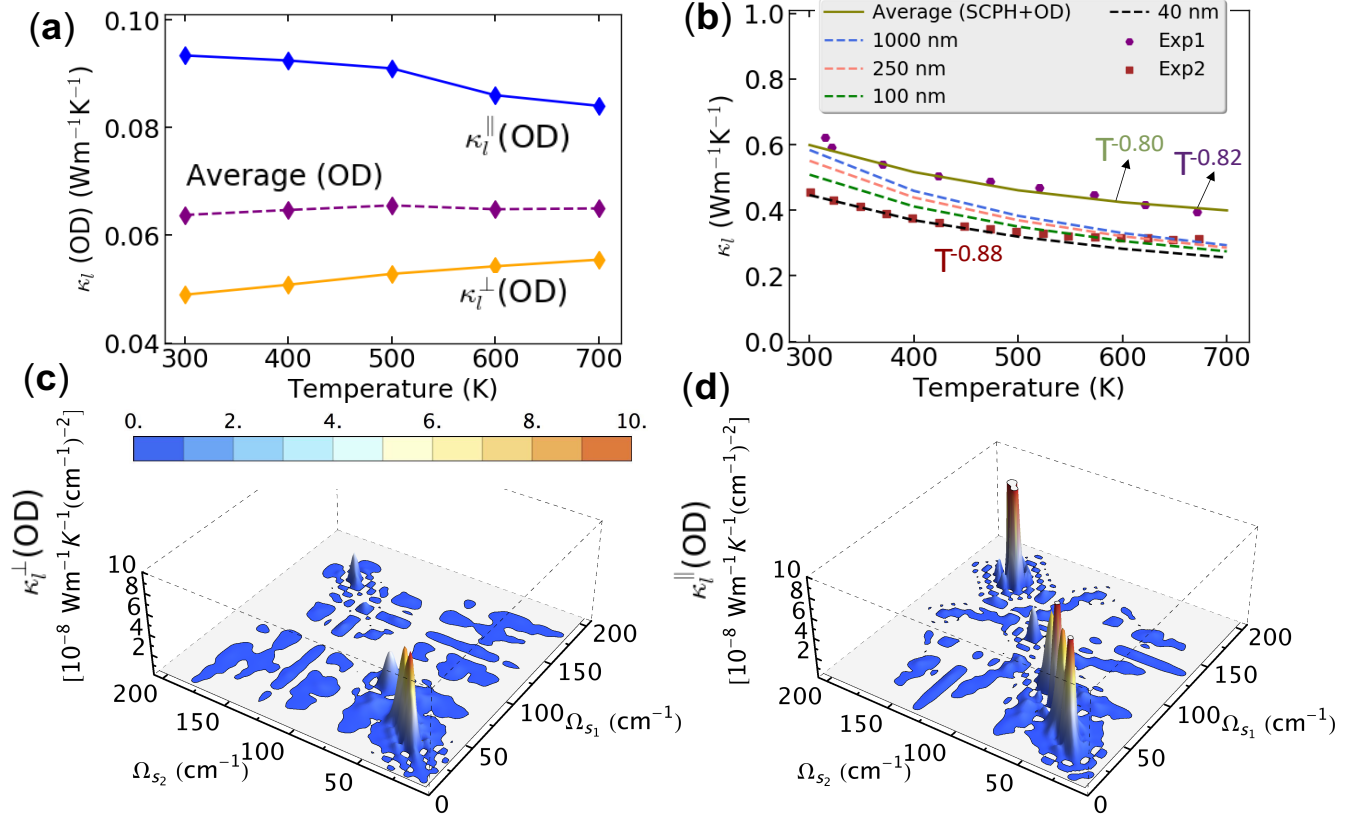


FIG. 4. Heat transport due to wave-like tunneling of phonons. (a) The off-diagonal (OD) contributions to κ_l (i.e., κ_l^{\parallel} , κ_l^{\perp} , and their average) calculated using the anharmonically renormalized phonon frequencies at each temperature. (b) Total κ_l (calculated within SCPH method) including the OD contributions reproduces the Exp1 [38] well. Additional grain-boundary scatterings on top of SCPH+OD contributions to κ_l reproduce Exp2 [39]. Grain sizes ranging from 40 to 1000 nm are considered here. Three-dimensional visualizations of the mode specific contributions to $\kappa_l(\text{OD})$ as a function of anharmonically renormalized phonon frequencies (i.e., Ω_s) at $T = 300$ K for the (c) κ_l^{\perp} and (d) κ_l^{\parallel} components. These quantities are plotted per cross-sectional area of the Brillouin zone to clearly highlight the phonon frequencies that primarily contribute to the $\kappa_l(\text{OD})$. A color scale corresponding to the variation of colors in Figs. 4c and 4d is shown, which has the same unit as indicated in the z-axes of both figures.

Effects of grain boundaries

Having reproduced the first set of experiments (i.e., Exp1 [38]), we notice that the measured κ_l of TiInTe_2 in another experiment (i.e., Exp2 [39]) is lower than the former. Since the measurements were performed in the polycrystalline samples of the compound in which the presence of grain boundaries are generally common, the lower κ_l in Exp2 [39] most likely originates from the additional scatterings of the heat carrying phonons due to the grain boundaries. We introduced grain-boundary scatterings on top of the three-phonon and isotope scatterings and calculated κ_l to see if this additional scattering mechanism can explain the second experiment (i.e., Exp2 [39]). Assuming that the boundary scatterings are predominantly diffuse, the grain-boundary scattering rates are given by $\tau_{\text{gb},\lambda}^{-1} = \frac{2|\mathbf{v}_{\lambda}|}{L}$, where \mathbf{v}_{λ} and L are the phonon group velocity and the averaged grain size, respectively.

The total scatterings rates of the phonons are obtained by applying the Matthiessen's rule, which are then used to calculate κ_l (see Supplementary Note 2 for details). We show in Fig. 4b the effect of grain boundary scatterings on κ_l as a function of grain size. It can be seen that κ_l is significantly modified in magnitudes particularly in low temperature (< 550 K). Our calculations show that while the phonon-scatterings due to the grains with an average size of 40 nm reproduce Exp2 [39] quite well below $T = 550$ K, larger grain sizes give rise to better agreement with Exp2 above 550 K (Fig. 4b).

DISCUSSION

After successfully explaining the experimental results, we now closely examine the mode-specific contributions to the $\kappa_l^{\perp}(\text{OD})$ and $\kappa_l^{\parallel}(\text{OD})$, which are shown in Fig. 4c and Fig. 4d, respectively, as three-dimensional plots av-

eraged over the planar area in the Brillouin zone. We see that phonons with very similar frequencies with $s_1 \neq s_2$ (i.e., near the diagonal in Fig. 4c) below 100 cm^{-1} primarily contribute to $\kappa_l^\perp(\text{OD})$. On the other hand, quasi-degenerate phonons in the frequency ranges of $20\text{-}100 \text{ cm}^{-1}$ and near 180 cm^{-1} mainly contribute to $\kappa_l^\parallel(\text{OD})$. It is interesting to note that the anisotropy (i.e., $\kappa_l^\parallel/\kappa_l^\perp$) of the PBTE calculated contributions ($\kappa_l(\text{SCPH})$) is much stronger than the anisotropy present in the $\kappa_l(\text{OD})$ contributions. For example, $\kappa_l^\parallel/\kappa_l^\perp = 2.6$ for the PBTE results while for the OD terms, $\kappa_l^\parallel/\kappa_l^\perp = 1.8$ at $T = 300 \text{ K}$. While the anisotropy in the phonon dispersion generally results in the anisotropy in κ_l obtained from PBTE as the group velocity in the PBTE is related to the single phonon mode, the much weaker anisotropy in $\kappa_l(\text{OD})$ stems from the fact that the OD heat transport takes place between coupled phonon eigenstates where the group velocity is associated with two different (quasi degenerate) frequencies. Thus, $\kappa_l(\text{OD})$ has a weak dependence on the slopes of the phonon branches, which partially counteracts the anisotropy in $\kappa_l(\text{PBTE})$. It is interesting to see that while $\kappa_l^\perp(\text{OD})$ increases with temperature, $\kappa_l^\parallel(\text{OD})$ decreases with temperature. Our analysis shows that this opposite temperature-dependence arises from the renormalization of the phonon frequencies at finite temperatures. We show in the Supplementary Figure 7 that when $\kappa_l^\perp(\text{OD})$ and $\kappa_l^\parallel(\text{OD})$ are calculated using the harmonic (i.e., $T = 0 \text{ K}$) phonon frequencies, both the components increase with temperature. However, we note that in all cases, the temperature-dependence of both components of $\kappa_l(\text{OD})$ are quite weak.

A previous attempt to understand the lattice thermal conductivity of TlInTe_2 was performed by Wu et al. [51] where the two-channel model [56] of thermal conductivity was used to explain the experimentally measured κ_l . The two-channel model has been invoked in cases where the particle-like description of phonons becomes insufficient to describe the observed κ_l of materials. Thus, a second channel of lattice heat conduction is introduced to compensate for the κ_l , which is attributed to arise from the localized hopping among the uncorrelated phonon oscillators [56]. In the two-channel model used by Wu et al. [51], the phonon frequencies were treated within the harmonic approximation ($T = 0 \text{ K}$) with no effects of temperature, which were then used to solve the particle-like contribution to κ_l using the PBTE. Hence, the calculated [51] κ_l underestimated the measured κ_l values of TlInTe_2 [38, 39]. To account for this difference, the contribution to κ_l coming from the second channel was calculated using the Cahill-Watson-Pohl (CWP) model [24] which estimates the minimum κ_l achievable in disordered solids. We note that our calculated κ_l within the unified theory that utilizes the anharmonically renormalized phonon frequencies successfully reproduces the experiments without requiring to invoke the second channel

of the two-channel model [56] of κ_l . Also, our calculated total κ_l shows better agreement with Exp1 [38] than the κ_l calculated using the two-channel model by Wu et al. [51] (see Supplementary Figure 4).

We note that we did not consider the effect the lattice thermal expansion in our calculations. In general, the thermal expansion will soften the phonon frequencies which give rise to the reduced phonon lifetimes and hence a lower- κ_l at high temperatures. However, this reduction is partially counterbalanced by the increase in the κ_l due to the anharmonic heat flux [46] at high temperature, which is also absent in the current formalism. We did not calculate the thermal expansion coefficient and the anharmonic heat flux of TlInTe_2 as their calculations are computationally very expensive for non-cubic lattice. Nonetheless, the interplay of the thermal expansion and anharmonic heat flux in TlInTe_2 and any ultralow- κ_l materials in general is worth exploring in future studies.

In summary, we have investigated the microscopic origin and the underlying physical principles governing the extremely low and weakly temperature-dependent lattice thermal conductivity in the chain-like crystalline semiconductor TlInTe_2 using a unified theory of lattice heat transport that combines both the particle-like propagation and wave-like tunneling of phonons. To treat the strong anharmonicity present in TlInTe_2 , we have applied the SCPH theory to anharmonically renormalize the phonon frequencies at finite temperatures considering the quartic anharmonicity. Our calculated κ_l using the PBTE coupled with the SCPH method (i.e., $\kappa_l(\text{SCPH})$) and the off-diagonal contributions (i.e., $\kappa_l(\text{OD})$) arising from the wave-like tunneling of phonons successfully reproduce both the magnitude and temperature dependence (milder than T^{-1} decay) of the measured κ_l in one set of experiments. Adding of additional grain-boundary scatterings on top of $\kappa_l(\text{SCPH}) + \kappa_l(\text{OD})$, our calculated κ_l reproduces well the second set of experiments. Our work thus highlights the important roles of (i) temperature induced renormalization of the harmonic phonon frequencies, particularly the low-energy rattling and other optical phonons, by the anharmonic effects, and (ii) the OD contributions to κ_l in the heat-flux operator to correctly explain the origin of unusual lattice thermal transport of strongly anharmonic solids. The detailed microscopic understanding of the heat transfer mechanism obtained in this work will provide guidance towards the rational design and discovery of hitherto unknown ultralow- κ_l compounds for various energy applications.

METHODS

Density functional theory calculations

We perform all density functional theory (DFT) calculations using the Vienna Ab-initio Simulation Pack-

age (VASP) [57, 58] employing the projector-augmented wave (PAW) [59] potentials of Tl ($5d^{10} 6s^2 6p^1$), In ($4d^{10} 5s^2 5p^1$) and Te ($5s^2 5p^4$) and utilized the PBEsol [60] parametrization of the generalized gradient approximation (GGA) [61] to the exchange-correlation energy functional. We use a kinetic energy cut-off of 520 eV, and Γ -centered k-point mesh of $12 \times 12 \times 12$ to sample the Brillouin zone. The fully optimized lattice constants ($a=8.406$ Å, $c=7.134$ Å) agree very well (absolute error < 1 %) with the experimentally reported values ($a=8.478$ Å, $c=7.185$ Å) [62]. We choose the high-symmetry k-path in the Brillouin zone while plotting the phonon dispersion following the convention of Setyawan et al. [63]. Phonon dispersions are calculated using the second-order interatomic force constants (IFCs) using Phonopy [64]. Since the calculated phonon scattering rates strongly depends on the phonon frequencies which can be quite sensitive to the supercell size, we have performed convergence tests (see Supplementary Figure 1), and adopted $2 \times 2 \times 2$ supercell for the calculations of the second-order IFCs.

Thermal conductivity calculations

To renormalize the phonon frequencies at finite temperature, and to calculate the lattice thermal conductivity (κ_l) using the PBTE, an accurate estimation of anharmonic IFCs, namely the third-order and fourth-order IFCs are required. We obtain these anharmonic IFCs using the compressive sensing lattice dynamics (CSLD) method [28, 29, 65, 66] using $2 \times 2 \times 2$ supercell and $6 \times 6 \times 6$ Γ -centered k-point mesh. While constructing the third and fourth order IFCs, a cut-off radius (r_c) is chosen, above which all three-body and four-body atomic interactions are discarded, respectively. Although with the increasing order of the IFCs, the atomic interactions become very short ranged, the value of r_c can be quite critical in correctly calculating κ_l [15]. We have performed convergence tests of κ_l against r_c (see Supplementary Figure 3) which are chosen to be 7.56 Å and 4 Å for the third and fourth-order IFCs, respectively. The r_c value for the third-order IFCs is carefully examined to give good convergence in the calculated κ_l . While we have calculated the particle-like contributions to κ_l using the PBTE considering the three-phonon, isotope and grain-boundary scatterings (see Supplementary Note 2 for details), the off-diagonal contributions to κ_l has been calculated by explicitly evaluating the off-diagonal terms of the heat-flux operator (see Supplementary Note 3 for details). Both these terms have been calculated by utilizing the anharmonically renormalized phonon frequencies obtained at finite temperatures.

Self-consistent phonon calculations

We solved the SCPH equations self-consistently until the phonon frequencies are converged to a given small threshold (e.g., 10^{-3} cm $^{-1}$). using a relatively dense $6 \times 6 \times 6$ mesh of \mathbf{q} -points. The renormalized phonon frequencies and eigenvectors are then used to obtain the renormalized harmonic IFCs through the inverse Fourier transformation. These renormalized IFCs are utilized to calculate phonon dispersions at finite temperatures. We note that in this study we did not take into account the second-order correction to ω_λ due to the cubic anharmonic term because their contributions have been found less significant than the phonon frequency hardening by the quartic anharmonicity in some of the low- κ_l systems such as PbTe [67] and clathrates [30]. However, we note that there are complex compounds like the tetrahedrites where the role of the cubic anharmonicity is found to be quite significant [35]. We calculate the particle-like contributions, κ_l (PBTE), by iteratively solving the PBTE using the ShengBTE code [44]. We use $12 \times 12 \times 12$ \mathbf{q} -point mesh to obtain κ_l with good convergence (see Figs. S3c-d). We present two components of the κ_l in the results section: κ_l^\parallel and κ_l^\perp , which are parallel and perpendicular to the InTe $_4$ chain direction (i.e., along the c-axis in Fig. 1a) in the crystal structure of TlInTe $_2$, respectively. While κ_l^\parallel is the zz-component of the κ_l -tensor, κ_l^\perp is the directional average of the xx and yy-components of the κ_l -tensor. The average κ_l is defined as the directional average of xx, yy and zz components of the κ_l -tensor throughout the manuscript. The $T^{-\alpha}$ fitting of the experimentally measured and calculated κ_l data of TlInTe $_2$ are shown in Supplementary Figure 5.

ACKNOWLEDGEMENTS

We acknowledge financial supports from the Department of Energy, Office of Science, Basic Energy Sciences under grant DE-SC0014520 (thermal conductivity calculations), and the U.S. Department of Commerce and National Institute of Standards and Technology as part of the Center for Hierarchical Materials Design (CHiMaD) under award no. 70NANB14H012 (DFT calculations). One of us (Y.X.) is partially supported by the Toyota Research Institute (TRI) through the Accelerated Materials Design and Discovery program (theory of anharmonic phonons). K.P. thanks Shashwat Anand for constructive comments on the manuscript. This work used computing resources provided by the (a) National Energy Research Scientific Computing Center (NERSC), a U.S. Department of Energy Office of Science User Facility operated under Contract No. DE-AC02-05CH11231, (b) the Extreme Science and Engineering Discovery Environment (National Science Foundation Contract ACI-1548562),

and (c) Quest high-performance computing facility at Northwestern University which is jointly supported by the Office of the Provost, the Office for Research, and Northwestern University Information Technology.

-
- [1] L. E. Bell, Cooling, heating, generating power, and recovering waste heat with thermoelectric systems, *Science* **321**, 1457 (2008).
 - [2] G. J. Snyder and E. S. Toberer, Complex thermoelectric materials, *Nat. Mater.* **7**, 105 (2008).
 - [3] D. G. Cahill, P. V. Braun, G. Chen, D. R. Clarke, S. Fan, K. E. Goodson, P. Keblinski, W. P. King, G. D. Mahan, A. Majumdar, H. J. Maris, S. R. Phillpot, E. Pop, and S. Li, Nanoscale thermal transport. ii. 2003–2012, *App. Phys. Rev.* **1**, 011305 (2014).
 - [4] X. Zhou, Y. Yan, X. Lu, H. Zhu, X. Han, G. Chen, and Z. Ren, Routes for high-performance thermoelectric materials, *Mater. Today* **21**, 974 (2018).
 - [5] M. A. Green and S. P. Bremner, Energy conversion approaches and materials for high-efficiency photovoltaics, *Nat. Mater.* **16**, 23 (2017).
 - [6] H. Xie, S. Hao, J. Bao, T. J. Slade, G. J. Snyder, C. Wolverton, and M. G. Kanatzidis, All-inorganic halide perovskites as potential thermoelectric materials: Dynamic cation off-centering induces ultralow thermal conductivity, *J. Am. Chem. Soc.* **142**, 9553 (2020).
 - [7] W. Lee, H. Li, A. B. Wong, D. Zhang, M. Lai, Y. Yu, Q. Kong, E. Lin, J. J. Urban, J. C. Grossman, and P. Yang, Ultralow thermal conductivity in all-inorganic halide perovskites, *Proc. Nat. Acad. Sci.* **114**, 8693 (2017).
 - [8] P. Acharyya, T. Ghosh, K. Pal, K. Kundu, K. Singh Rana, J. Pandey, A. Soni, U. V. Waghmare, and K. Biswas, Intrinsically ultralow thermal conductivity in ruddlesden-popper 2d perovskite $\text{Cs}_2\text{PbI}_2\text{Cl}_2$: Localized anharmonic vibrations and dynamic octahedral distortions, *J. Am. Chem. Soc.* **142**, 1559515603 (2020).
 - [9] R. Darolia, Thermal barrier coatings technology: critical review, progress update, remaining challenges and prospects, *Int. Mater. Rev.* **58**, 315 (2013).
 - [10] T. Matsunaga, N. Yamada, R. Kojima, S. Shamoto, M. Sato, H. Tanida, T. Uruga, S. Kohara, M. Takata, P. Zalden, G. Bruns, I. S. H. C. Wille, R. P. Hermann, and M. Wuttig, Phase-change materials: vibrational softening upon crystallization and its impact on thermal properties, *Adv. Funct. Mater.* **21**, 2232 (2011).
 - [11] W. Li, S. Lin, B. Ge, J. Yang, W. Zhang, and Y. Pei, Low sound velocity contributing to the high thermoelectric performance of Ag_8SnSe_6 , *Adv. Sci.* **3**, 1600196 (2016).
 - [12] Y. Shi, A. Assoud, S. Ponou, S. Lidin, and H. Kleinke, A new material with a composite crystal structure causing ultralow thermal conductivity and outstanding thermoelectric properties: $\text{Ti}_2\text{Ag}_{12}\text{Te}_{7+\delta}$, *J. Am. Chem. Soc.* **140**, 8578 (2018).
 - [13] W. Peng, G. Petretto, G.-M. Rignanese, G. Hautier, and A. Zevalkink, An unlikely route to low lattice thermal conductivity: Small atoms in a simple layered structure, *Joule* **2**, 1879 (2018).
 - [14] M. Christensen, A. B. Abrahamsen, N. B. Christensen, F. Juranyi, N. H. Andersen, K. Lefmann, J. Andreasson, C. R. Bahl, and B. B. Iversen, Avoided crossing of rattler modes in thermoelectric materials, *Nat. Mater.* **7**, 811 (2008).
 - [15] C. W. Li, J. Hong, A. F. May, D. Bansal, S. Chi, T. Hong, G. Ehlers, and O. Delaire, Orbital driven giant phonon anharmonicity in SnSe , *Nat. Phys.* **11**, 1063 (2015).
 - [16] M. D. Nielsen, V. Ozolins, and J. P. Heremans, Lone pair electrons minimize lattice thermal conductivity, *Energy Environ. Sci.* **6**, 570 (2013).
 - [17] Y. Zhang, E. Skoug, J. Cain, V. Ozoliņš, D. Morelli, and C. Wolverton, First-principles description of anomalously low lattice thermal conductivity in thermoelectric Cu_2SbSe ternary semiconductors, *Phys. Rev. B* **85**, 054306 (2012).
 - [18] K. Pal, Y. Xia, J. He, and C. Wolverton, Intrinsically low lattice thermal conductivity derived from rattler cations in an Ag_3SbS_3 family of chalcogenides, *Chem. Mater.* **31**, 8734 (2019).
 - [19] J. M. Skelton, L. A. Burton, S. C. Parker, A. Walsh, C.-E. Kim, A. Soon, J. Buckeridge, A. A. Sokol, C. R. A. Catlow, A. Togo, and I. Tanaka, Anharmonicity in the high-temperature Cu_2SbSe phase of SnSe : Soft modes and three-phonon interactions, *Phys. Rev. Lett.* **117**, 075502 (2016).
 - [20] W. Qiu, L. Xi, P. Wei, X. Ke, J. Yang, and W. Zhang, Part-crystalline part-liquid state and rattling-like thermal damping in materials with chemical-bond hierarchy, *Proc. Natl. Acad. Sci.* **111**, 15031 (2014).
 - [21] Y. Zhou and L.-D. Zhao, Promising thermoelectric bulk materials with 2d structures, *Adv. Mater.* **29**, 1702676 (2017).
 - [22] K. Pal, J. He, and C. Wolverton, Bonding hierarchy gives rise to high thermoelectric performance in layered zintl compound BaAu_2P_4 , *Chem. Mater.* (2018).
 - [23] M. Samanta, K. Pal, U. V. Waghmare, and K. Biswas, Intrinsically low thermal conductivity and high carrier mobility in dual topological quantum material, n -type BiTe , *Angew. Chem.* **132**, 4852 (2020).
 - [24] D. G. Cahill, S. K. Watson, and R. O. Pohl, Lower limit to the thermal conductivity of disordered crystals, *Phys. Rev. B* **46**, 6131 (1992).
 - [25] P. B. Allen and J. L. Feldman, Thermal conductivity of disordered harmonic solids, *Phys. Rev. B* **48**, 12581 (1993).
 - [26] P. B. Allen and J. L. Feldman, Thermal conductivity of glasses: Theory and application to amorphous Si , *Phys. Rev. Lett.* **62**, 645 (1989).
 - [27] T. Sun and P. B. Allen, Lattice thermal conductivity: Computations and theory of the high-temperature breakdown of the phonon-gas model, *Phys. Rev. B* **82**, 224305 (2010).
 - [28] F. Zhou, W. Nielson, Y. Xia, and V. Ozoliņš, Lattice anharmonicity and thermal conductivity from compressive sensing of first-principles calculations, *Phys. Rev. Lett.* **113**, 185501 (2014).
 - [29] T. Tadano and S. Tsuneyuki, Self-consistent phonon calculations of lattice dynamical properties in cubic SrTiO_3 with first-principles anharmonic force constants, *Phys. Rev. B* **92**, 054301 (2015).
 - [30] T. Tadano and S. Tsuneyuki, Quartic anharmonicity of rattlers and its effect on lattice thermal conductivity of clathrates from first principles, *Phys. Rev. Lett.* **120**,

- 105901 (2018).
- [31] I. Errea, B. Rousseau, and A. Bergara, Anharmonic stabilization of the high-pressure simple cubic phase of calcium, *Phys. Rev. Lett.* **106**, 165501 (2011).
 - [32] M. Simoncelli, N. Marzari, and F. Mauri, Unified theory of thermal transport in crystals and glasses, *Nat. Phys.* **15**, 809 (2019).
 - [33] L. Isaeva, G. Barbalinardo, D. Donadio, and S. Baroni, Modeling heat transport in crystals and glasses from a unified lattice-dynamical approach, *Nat. Comm.* **10**, 1 (2019).
 - [34] J. Klarbring, O. Hellman, I. A. Abrikosov, and S. I. Simak, Anharmonicity and ultralow thermal conductivity in lead-free halide double perovskites, *Phys. Rev. Lett.* **125**, 045701 (2020).
 - [35] Y. Xia, V. Ozoliņš, and C. Wolverton, Microscopic mechanisms of glasslike lattice thermal transport in cubic $\text{Cu}_{12}\text{Sb}_4\text{S}_{13}$ tetrahedrites, *Phys. Rev. Lett.* **125**, 085901 (2020).
 - [36] Y. Xia, K. Pal, J. He, V. Ozoliņš, and C. Wolverton, Particlelike phonon propagation dominates ultralow lattice thermal conductivity in crystalline Ti_3VSe_4 , *Phys. Rev. Lett.* **124**, 065901 (2020).
 - [37] I. Errea, M. Calandra, C. J. Pickard, J. Nelson, R. J. Needs, Y. Li, H. Liu, Y. Zhang, Y. Ma, and F. Mauri, High-pressure hydrogen sulfide from first principles: A strongly anharmonic phonon-mediated superconductor, *Phys. Rev. Lett.* **114**, 157004 (2015).
 - [38] H. Matsumoto, K. Kurosaki, H. Muta, and S. Yamanaka, Systematic investigation of the thermoelectric properties of TMTe_2 ($\text{M} = \text{Ga, In, or Tl}$), *J. Appl. Phys.* **104**, 073705 (2008).
 - [39] M. K. Jana, K. Pal, A. Warankar, P. Mandal, U. V. Waghmare, and K. Biswas, Intrinsic rattler-induced low thermal conductivity in ZnTe type TMTe_2 , *J. Am. Chem. Soc.* **139**, 4350 (2017).
 - [40] M. K. Jana, K. Pal, U. V. Waghmare, and K. Biswas, The origin of ultralow thermal conductivity in InTe : Lone-pair-induced anharmonic rattling, *Angew. Chem., Int. Ed.* **55**, 7792 (2016).
 - [41] M. Dutta, S. Mattepanavar, M. V. Prasad, J. Pandey, A. Warankar, P. Mandal, A. Soni, U. V. Waghmare, and K. Biswas, Ultralow thermal conductivity in chain-like TeSe_2 due to inherent Te^{2+} rattling, *J. Am. Chem. Soc.* **141**, 20293 (2019).
 - [42] T. Tadano, Y. Gohda, and S. Tsuneyuki, Impact of rattlers on thermal conductivity of a thermoelectric clathrate: A first-principles study, *Phys. Rev. Lett.* **114**, 095501 (2015).
 - [43] W. Li and N. Mingo, Ultralow lattice thermal conductivity of the fully filled skutterudite $\text{YbFe}_4\text{Sb}_{12}$ due to the flat avoided-crossing filler modes, *Phys. Rev. B* **91**, 144304 (2015).
 - [44] W. Li, J. Carrete, N. A. Katcho, and N. Mingo, ShengBTE: A solver of the Boltzmann transport equation for phonons, *Comp. Phys. Comm.* **185**, 1747 (2014).
 - [45] A. van Rooykeghem, J. Carrete, C. Oses, S. Curtarolo, and N. Mingo, High-throughput computation of thermal conductivity of high-temperature solid phases: the case of oxide and fluoride perovskites, *Phys. Rev. X* **6**, 041061 (2016).
 - [46] R. J. Hardy, Energy-flux operator for a lattice, *Phys. Rev.* **132**, 168 (1963).
 - [47] P. B. Allen, J. L. Feldman, J. Fabian, and F. Wooten, Diffusons, locons and propagons: Character of atomic vibrations in amorphous Si, *Phil. Mag. B* **79**, 1715 (1999).
 - [48] W. Lv and A. Henry, Non-negligible contributions to thermal conductivity from localized modes in amorphous silicon dioxide, *Sci. Rep.* **6**, 1 (2016).
 - [49] G. Kané, M. Lazzeri, and F. Mauri, Zener tunneling in the electrical transport of quasimetallic carbon nanotubes, *Phys. Rev. B* **86**, 155433 (2012).
 - [50] L.-D. Zhao, S.-H. Lo, Y. Zhang, H. Sun, G. Tan, C. Uher, C. Wolverton, V. P. Dravid, and M. G. Kanatzidis, Ultralow thermal conductivity and high thermoelectric figure of merit in SnSe crystals, *Nature* **508**, 373 (2014).
 - [51] M. Wu and L. Huang, Unusual lattice thermal conductivity in the simple crystalline compounds TMTe_2 ($\text{x} = \text{Ga, In}$), *Phys. Rev. B* **100**, 075207 (2019).
 - [52] R. Cowley, Anharmonic crystals, *Rep. Prog. Phys.* **31**, 123 (1968).
 - [53] N. Werthamer, Self-consistent phonon formulation of anharmonic lattice dynamics, *Phys. Rev. B* **1**, 572 (1970).
 - [54] M. Klein and G. Horton, The rise of self-consistent phonon theory, *J. Low Temp. Phys.* **9**, 151 (1972).
 - [55] S. Pailhès, H. Euchner, V. M. Giordano, R. Debord, A. Assy, S. Gomès, A. Bosak, D. Machon, S. Paschen, and M. De Boissieu, Localization of propagative phonons in a perfectly crystalline solid, *Phys. Rev. Lett.* **113**, 025506 (2014).
 - [56] S. Mukhopadhyay, D. S. Parker, B. C. Sales, A. A. Puretzy, M. A. McGuire, and L. Lindsay, Two-channel model for ultralow thermal conductivity of crystalline Ti_3VSe_4 , *Science* **360**, 1455 (2018).
 - [57] G. Kresse and J. Furthmüller, Efficiency of ab-initio total energy calculations for metals and semiconductors using a plane-wave basis set, *Comp. Mater. Sci.* **6**, 15 (1996).
 - [58] G. Kresse and J. Furthmüller, Efficient iterative schemes for ab initio total-energy calculations using a plane-wave basis set, *Phys. Rev. B* **54**, 11169 (1996).
 - [59] G. Kresse and D. Joubert, From ultrasoft pseudopotentials to the projector augmented-wave method, *Phys. Rev. B* **59**, 1758 (1999).
 - [60] J. P. Perdew, A. Ruzsinszky, G. I. Csonka, O. A. Vydrov, G. E. Scuseria, L. A. Constantin, X. Zhou, and K. Burke, Restoring the density-gradient expansion for exchange in solids and surfaces, *Phys. Rev. Lett.* **100**, 136406 (2008).
 - [61] J. P. Perdew, K. Burke, and M. Ernzerhof, Generalized gradient approximation made simple, *Phys. Rev. Lett.* **77**, 3865 (1996).
 - [62] J. Bannys, F. Wondre, and G. Guseinov, Powder diffraction study of TiGeTe_2 , TiTe_2 and TiInSe_2 , *Mater. Lett.* **9**, 269 (1990).
 - [63] W. Setyawan and S. Curtarolo, High-throughput electronic band structure calculations: Challenges and tools, *Comp. Mater. Sci.* **49**, 299 (2010).
 - [64] A. Togo and I. Tanaka, First principles phonon calculations in materials science, *Scr. Mater.* **108**, 1 (2015).
 - [65] F. Zhou, W. Nielson, Y. Xia, and V. Ozoliņš, Compressive sensing lattice dynamics. i. general formalism, *Physical Review B* **100**, 184308 (2019).
 - [66] F. Zhou, B. Sadigh, D. Åberg, Y. Xia, and V. Ozoliņš, Compressive sensing lattice dynamics. ii. efficient phonon calculations and long-range interactions, *Physical Review B* **100**, 184309 (2019).
 - [67] Y. Xia, Revisiting lattice thermal transport in PbTe : The crucial role of quartic anharmonicity, *App. Phys. Lett.*

113, 073901 (2018).